Regional chemical weather forecasting system CFORS: Model descriptions and analysis of surface observations at Japanese island stations during the ACE-Asia experiment

I. Uno,[1,2] G. R. Carmichael,[3] D. G. Streets,[4] Y. Tang,[3] J. J. Yienger,[5] S. Satake,[1] Z. Wang,[2] Jung-Hun Woo,[3] S. Guttikunda,[3] M. Uematsu,[6] K. Matsumoto,[6,7] H. Tanimoto,[8] K. Yoshioka,[9] and T. Iida[10]

Received 14 August 2002; revised 25 March 2003; accepted 17 April 2003; published 7 August 2003.

[1] The Chemical Weather Forecast System (CFORS) is designed to aid in the design of field experiments and in the interpretation/postanalysis of observed data. The system integrates a regional chemical transport model with a multitracer, online system built within the Regional Atmospheric Modeling System (RAMS) mesoscale model. CFORS was deployed in forecast and postanalysis modes during the NASA Global Tropospheric Experiment (GTE)-Transport and Chemical Evolution over the Pacific (TRACE-P), International Global Atmospheric Chemistry project (IGAC)-International Geosphere-Biosphere Programme (IGBP) Asian Pacific Regional Aerosol Characterization Experiment (ACE-Asia), and National Oceanic and Atmospheric Administration Intercontinental Transport and Chemical Transformation of Anthropogenic Pollution 2002 (ITCT 2K2) field studies. A description of the CFORS model system is presented. The model is used to help interpret the Variability of Maritime Aerosol Properties (VMAP) surface observation data. The CFORS model results help to explain the time variation of both anthropogenic pollutants (sulfate, black carbon, and CO) and natural constituents including radon and mineral dust. Time series and time-height cross-section analysis of gases and aerosols are presented to help identify key processes. Synoptic-scale weather changes are found to play an important role in the continental-scale transport of pollution in the springtime in East Asia. The complex vertical and horizontal structure of pollutants in these outflow events is also presented and discussed. *INDEX TERMS:* 0305 Atmospheric Composition and Structure: Aerosols and particles (0345, 4801); 0345 Atmospheric Composition and Structure: Pollution—urban and regional (0305); 0365 Atmospheric Composition and Structure: Troposphere—composition and chemistry; *KEYWORDS:* chemical transport model, dust, aerosol, ACE-Asia, observation, aerosol optical thickness

Citation: Uno, I., et al., Regional chemical weather forecasting system CFORS: Model descriptions and analysis of surface observations at Japanese island stations during the ACE-Asia experiment, *J. Geophys. Res.*, *108*(D23), 8668, doi:10.1029/2002JD002845, 2003.

1. Introduction

[2] Large-scale intensive field experiments play an important role in atmospheric chemistry research, as exemplified by the recent NASA Global Tropospheric Experiment (GTE)-Transport and Chemical Evolution over the Pacific (TRACE-P) [*Jacob et al.*, 2003], International Global Atmospheric Chemistry project (IGAC)-International Geosphere-Biosphere Programme (IGBP) Asian Pacific Regional Aerosol Characterization Experiment (ACE-Asia) [*Huebert et al.*, 2003] and National Oceanic and Atmospheric Administration (NOAA) Intercontinental Transport and Chemical Transformation of Anthropogenic Pollution 2002 (ITCT 2K2) studies. These experiments involved multiple aircraft, ships, satellite measurements, ground-based observations, and engaged more than 100 scientists. They were designed to characterize atmospheric chemistry and transport in association with features of specific scientific interest (e.g., transport of pollutants in association with postfrontal

[1]Research Institute for Applied Mechanics, Kyushu University, Kasuga, Japan.
[2]Frontier Research System for Global Change, Yokohama, Japan.
[3]Center for Global and Regional Environmental Research, University of Iowa, Iowa City, Iowa, USA.
[4]Argonne National Laboratory, Argonne, Illinois, USA.
[5]Cities for Climate Protection Campaign, International Council for Local Environmental Initiatives, U.S. Office, Berkeley, California, USA.
[6]Ocean Research Institute, University of Tokyo, Tokyo, Japan.
[7]Japan Science and Technology Corporation, Tokyo, Japan.
[8]National Institute for Environmental Studies, Tsukuba, Japan.
[9]Shimane Prefectural Institute of Public Health and Environmental Science, Matsue, Japan.
[10]Graduate School of Engineering, Nagoya University, Nagoya, Japan.

0148-0227/03/2002JD002845$09.00

outflow) and to test certain aspects of our understanding. One difficulty in the execution of such experiments lies in the fact that features of interests are usually transient in nature. Flight planning relies on forecasting what features of interest are in the region and where they are expected to be at the time of the flight. Traditionally, flight planning has relied on meteorological forecasts alone. Chemical transport models (CTMs) are now being used in forecast-mode to enhance flight planning by enabling the representation of important three-dimensional atmospheric chemical structures (such as dust storm plumes, polluted air masses associated with large cities, and widespread biomass burning events) and how they evolve over time. For example, *Lee et al.* [1997] and *Flatoy et al.* [2000] focused on a regional chemical weather forecasting system, while *Lawrence et al.* [2003] showed the model system for a global application. With this added information, it is hoped that the expensive field-deployed resources (facilities and people) can be employed/utilized more effectively, and science successes maximized.

[3] CTM forecasts play the additional important role of providing a contextual representation of the experiment, and facilitate a quick analysis of the field results. The data obtained along the flight tracks for specific experiments (of typical duration of 8 hours) provide the "real" representation of the atmosphere at those specific points in time and space. The models predict the time evolution and three-dimensional structures within the entire region of operation during the proposed measurement period. When measured and modeled data are viewed together, the context of the observations is elucidated. For example, one can see the sources of the air mass intercepted and measured by the aircraft and where it was headed. In addition, when viewed over the entire field period (typically weeks to months), the combined data set of measured and modeled quantities allows for an assessment of how typical the observed features are (i.e., is the observed feature unusual or do events like it occur with some regularity) [*Ehhalt et al.*, 1997; *Lawrence*, 2001].

[4] We developed an operational Chemical Weather Forecasting System (CFORS) based on a 3-D online regional-scale chemical transport model fully coupled with the Regional Atmospheric Modeling System (RAMS) [*Pielke et al.*, 1992] to support atmospheric chemistry field experiments. CFORS was applied in the design and execution of the ACE-Asia and TRACE-P intensive field experiments. In this paper, we present a detailed description of the CFORS chemical transport model and illustrate the performance of CFORS using observations from two Japanese islands. A detailed analysis of the aircraft measurements during ACE-Asia is described by G. R. Carmichael et al. (Overview of regional scale analysis of aircraft data during ACE-Asia, manuscript in preparation, 2003). Illustrated examples of the use of CFORS for flight planning are presented by *Carmichael et al.* [2003b].

2. Description of CFORS

2.1. General Concept of RAMS/CFORS System

[5] Analysis of the long-range transport of pollution requires meteorological information (e.g., 3-D winds, boundary-layer (BL) turbulence, surface fluxes, cloud and precipitation) with high temporal and spatial resolution. Global data sets are available from several sources including: ECMWF (European Center for Medium Range Weather Forecasting); NCEP (NOAA National Center for Environmental Prediction); and JMA (Japan Meteorological Agency). These archived data sets typically have spatial resolution of $\sim$1–2 deg in latitude and longitude and 6 hour time interval. For regional-scale applications meteorological information is needed with higher resolution. The current generation of regional chemical/transport models recalculates meteorological fields using mesoscale meteorological models. For example, the U.S. EPA Community Multi-Scale Air Quality (CMAQ) [*Ching and Byun*, 1999] model uses the output from the NCAR/Penn State Mesoscale Model version 5 (MM5).

[6] CFORS is designed as a multitracer, online, system built within the Regional Atmospheric Modeling System (RAMS) [*Pielke et al.*, 1992]. (Here we refer to online in terms of calculating the tracers inside the meteorological model. In the present version we do not include the feedbacks of the tracer fields on the meteorology.) A unique feature of CFORS is that multiple tracers are run online in RAMS, so that all the meteorological information from RAMS is directly used by the tracer model at every time step ($\sim$90 sec). As a result, CFORS produces with high-time-resolution 3-dimensional fields of tracer distributions and major meteorological parameters. CFORS builds upon the online transport module for mineral dust and SO_2 in RAMS reported by *Uno et al.* [2001].

[7] CFORS is a flexible system with many possible configurations. Table 1 summarizes the RAMS options used in CFORS in support of ACE-Asia, TRACE-P and ITCT-2K2 experiments. In the results presented here, the Kuo cumulus parameterization was used to represent the subgrid-scale cumulus convection along with Kessler-type microphysics [*Walko et al.*, 1995]. The microphysics module in RAMS is capable of simulating mesoscale clouds and precipitation phenomena. The surface flux calculation module in RAMS [*Louis*, 1979] was improved on the basis of the results of *Uno et al.* [1995]. The level 2.5 turbulent closure model [*Mellor and Yamada*, 1974] and Land Ecosystem Atmosphere Feedback model (LEAF) [*Lee*, 1992] soil-vegetation model were also used.

Table 1. Specification of RAMS Parameters Used in the CFORS

Model Modules	Description
Basic equations	Non-hydrostatic; compressible
Horizontal coordinates	Rotated polar-sterographics (center 25°N and 115°N; horizonal grid spacing 80 km)
Vertical coordinates	Terrain-following σ_z (22 vertical levels from surface to 23 km)
Explicit microphysics	*Walko et al.* [1995]
Surface flux	*Louis* [1979] and *Uno et al.* [1995]
Radiation	*Chen and Cotton* [1983]
Turbulence	Horizontal: Smagorinsk deformation Vertical: *Mellor and Yamada* [1982] Level 2.5 turbulent closure
Cumulus convection	simplified Kuo scheme [*Tremback*, 1990]
Vegetation	LEAF2 [*Lee*, 1992]
Time marching	Hybrid scheme
Advection scheme	second-order upwind (positive definite scheme for scalar variable)
Integration time step	90 sec

Table 2. List of Parameters Included in the RAMS/CFORS System[a]

CTM Species	First-Order Reaction, %/h	Deposition (Sea/Land), m/s	Wet Scavenging, s^{-1}	Emission Reference[b]	Web Site[c]
SO_2	−1.0 (to SO_4)	3E-3/3E-3	2.0E-5 × Pr	S	O
SO_4	+1.0 (from SO_2)	1E-3/2E-3	5.5E-5× $Pr^{0.88}$		O
Black Carbon	–	1E-4/1E-3	–	S	O
Organic Carbon	–	2E-4/2E-3	1E-6 × Pr	S	O
CO-anthropogenic	−0.08	0/0	–	S	O
CO-Biomass	−0.08	0/0	–	S	O
Slow HC (Ethane)	−0.045	0/0	–	S	O
Fast HC (Ethene)	−1.44	0/0	–	S	O
Sea Salt				online (G)	
fine (<2.5 μm)	–	1E-3/1E-3	5E-5 × Pr		O
coarse (> 2.5 μm)	–	5E-3/5E-3	6E-5 × $Pr^{0.83}$		O
^{222}Radon	−0.7	0/0	–	online (J)	O
Lightning NO_x	−3.3	1E-3/1E-3	–	online (P)	O
NO_x	−3.3	1E-3/1E-3	–	S	
Dust				online	O
D_p < 1 μm	–	5E-4/5E-4	1E-5 × Pr		
1 μm < D_p < 2.5 μm	–	3E-3/3E-3	1E-5 × Pr		
2.5 μm < D_p < 10 μm	–	1E-2/1E-2	6E-5 × $Pr^{0.83}$		
10 μm < D_p	–	1E-1/1E-1	6E-5 × $Pr^{0.83}$		
Volcano Tracer	–	0/0	–	F	O
Megaciy Tracer	–	0/0	–	S	O

[a]Tracers that include emission, reaction, and removal processes are indicated. Pr: precipitation rate in mm/h.
[b]S, *Streets et al.* [2003]; F. *Fujita et al.* [1992]; G, *Gong et al.* [1997]; P, *Pickering et al.* [1998]; and J, *Jacob et al.* [1997].
[c]On the web site we also placed the meteorological parameters (wind fields, temperature, humidity, precipitation, cloud, rain), the potential vorteicity and the aerosol optical depth.

[8] CFORS is designed for both meteorological and chemical forecasting. For use in the field experiments tracers were chosen to help characterize air masses. The tracers used in CFORS are listed in Table 2 and include (1) important anthropogenic species (SO_2/SO_4, CO, black carbon (BC), organic carbon (OC), fast and slow reacting hydrocarbons); (2) species of natural origin (mineral dust, sea salt, radon, volcanic SO_2); and (3) markers for biomass burning (CO, BC, and OC). Aerosol optical depths (AOD) for sulfate, BC, OC, sea salts, dust and total value are important and calculated in CFORS at 500 nm after *Takemura et al.* [2000]. Aerosol extinction coefficient and single scattering albedo (SSA) were also calculated to compare with observation data.

[9] For the applications discussed in this paper, CFORS did not include online calculation of photochemical processes. Rather, in the forecast applications for the field experiments we calculated photochemistry using off-line chemical/transport models (such as Sulfur Transport Eulerian Model (STEM) [*Carmichael et al.*, 1987] and CMAQ), which were driven by the RAMS/CFORS meteorology. Figure 1 shows the RAMS/CFORS daily operational cycle, and Figure 2 shows the general modeling flowchart of the RAMS/CFORS/STEM/CMAQ system that was used in TRACE-P postanalysis phase [*Carmichael et al.*, 2003b].

2.2. Description of Tracer Modules

[10] The mass conservation equation used in CFORS is as follows:

$$\rho_{air}\left\{\frac{\partial}{\partial t}q_a + div(q_a \cdot \mathbf{v})\right\} = F_{diff} + F_{grav} + F_{react} + F_{emis} + F_{dry} + F_{wet} \quad (1)$$

where ρ_{air} is the air density, q_a is the gas/aerosol mass mixing ratio and $\boldsymbol{v}$ is the 3-D wind velocity vector; F_{diff}, F_{grav}, F_{react}, F_{emis}, F_{dry} and F_{wet} are the turbulent diffusion, gravitational settling, chemical reaction/conversion, emission, and dry/wet deposition tendency of gas/aerosols, respectively. The F_{grav} process is included only when gravitational settling is important for aerosol mass budgets (i.e., mineral dust and sea salt). In forecasting applications we treat the aerosols as external mixtures, and ignore aerosol interaction and the growth processes.

[11] Numerical integration of chemical tracers is performed within the RAMS driver. We used a positive definite advection scheme for scalar variables (i.e., chemical tracers). The horizontal diffusivity for meteorological scalar variables (such as temperature and water vapor) in RAMS is large, so to reduce the numerical horizontal diffusion of tracers, we reduced the scalar diffusivity to 10% of the value for water vapor.

[12] Cumulus convection plays an important role for the vertical distribution of biomass burning sources in subtropical regions, such as southern China, Thailand and Myanmar. The vertical redistribution of tracers by cumulus activities was treated as enhanced vertical turbulent diffusivities from the bottom to top of the cumulus cloud layers as identified by the RAMS simplified Kuo cumulus scheme. An Arakawa C grid system is used for all of chemical scalars in the framework of RAMS.

[13] The main purpose of the CFORS chemical tracer model is to identify major features associated with outflow of pollutants emitted within Asia. Therefore all the initial concentrations of chemical tracers were set to zero. The inflow boundary concentrations were also set to zero. For the outflow condition, a zero gradient lateral boundary condition was applied.

[14] In the forecast model we used constant dry deposition velocities for land and water surface as listed in Table 2. Wet scavenging processes were applied as a function of surface precipitation rate Pr (mm/h) only below the cloud

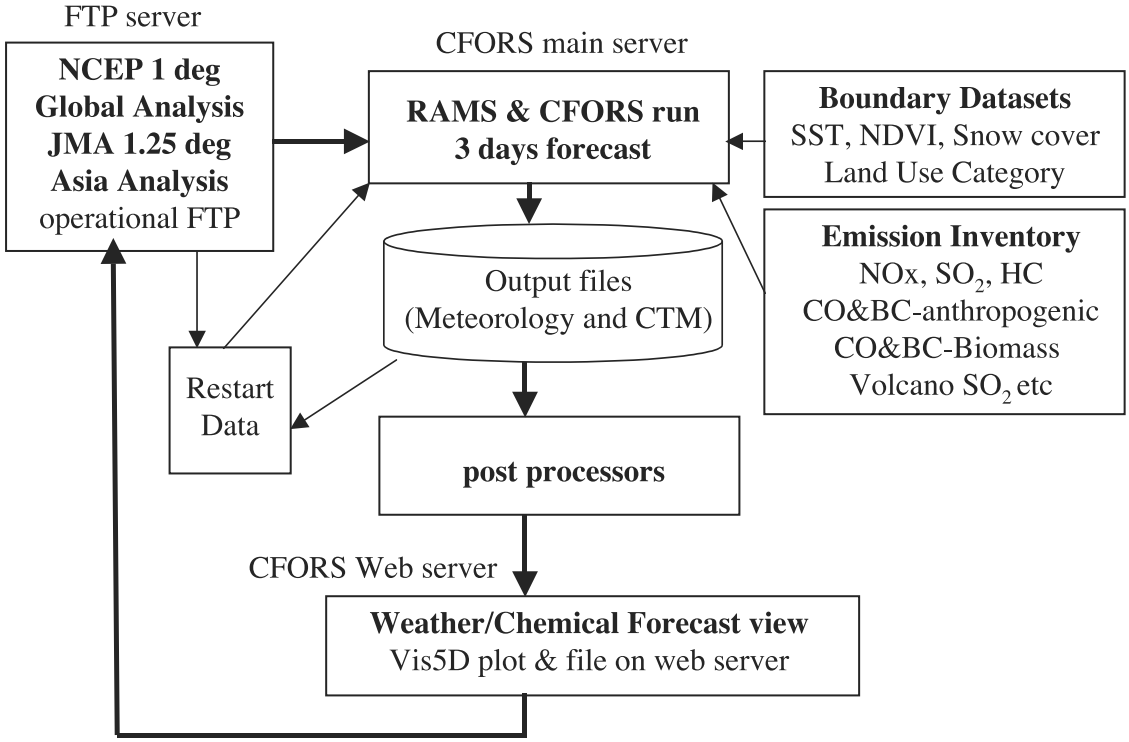

Figure 1. Schematic of the RAMS/CFORS daily operational cycle.

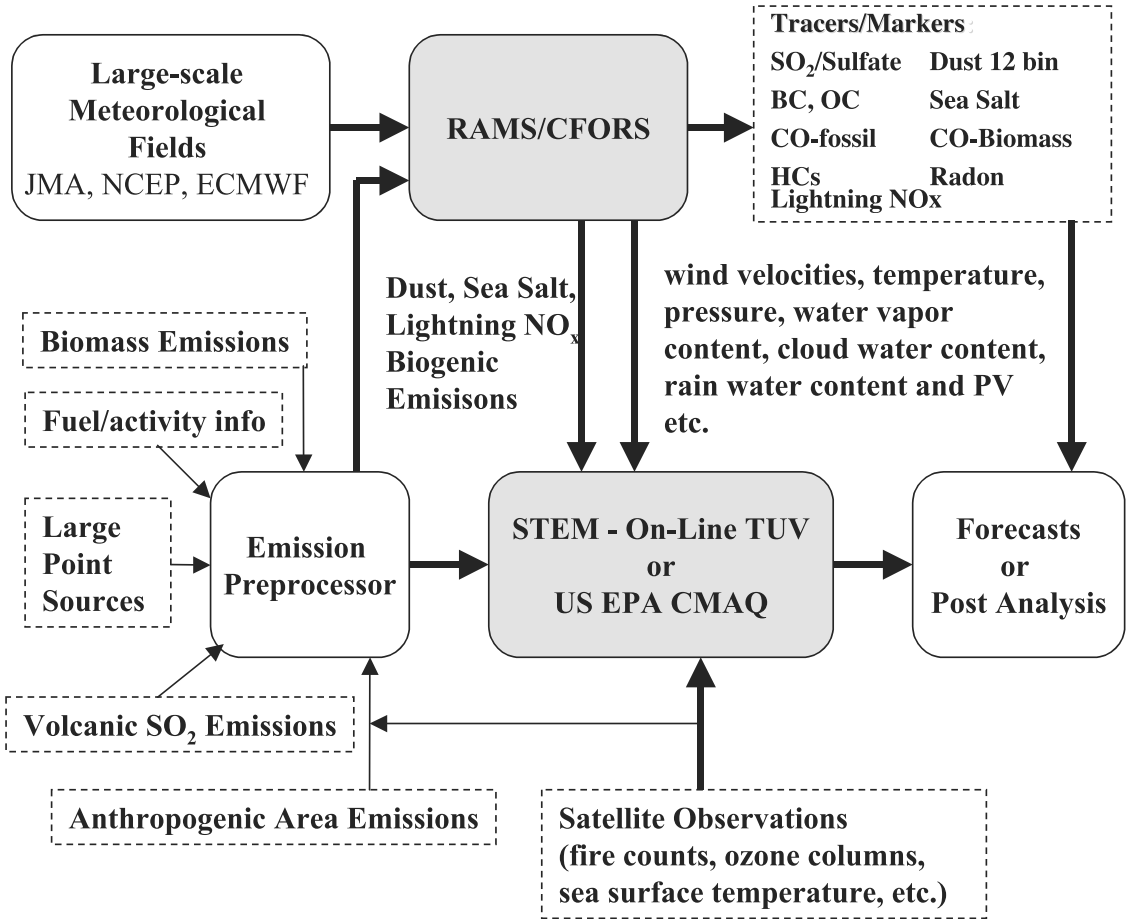

Figure 2. RAMS/CFORS/STEM/CMAQ postanalysis flowchart.

base height, and the cloud base was diagnosed from RAMS hydrometeor field. F_{wet} is given by,

$$F_{wet} = -C_1 \mathrm{Pr}^{C_2} \cdot q_a \cdot \rho_{air} \quad (2)$$

and C_1 and C_2 are the dimensionless parameters shown in Table 2.

2.2.1. Mineral Dust

[15] Forecasting and analysis of dust events is an important use of CFORS. Previous dust modeling work by *Uno et al.* [2001] assumed a single dust mode and assigned the dust flux as a function of surface wind speed. CFORS updates the dust module and treats size-resolved mineral dust using 12 particle size bins. The 12 size ranges are 0.1–0.16, 0.16–0.25, 0.25–0.40, 0.40–0.63, 0.63–1.00, 1.00–1.58, 1.58–2.51, 2.51–3.98, 3.98–6.31, 6.31–10.0, 10.0–15.85, 15.85–25.12 μm in radius, with corresponding effective radii of 0.13, 0.21, 0.33, 0.52, 0.82, 1.27, 2.01, 3.19, 4.06, 8.01, 12.7, 20.1 μm, respectively. The mass distribution varies linearly with respect to radius ($r < 1.0$ μm) and to log(radius) ($r > 1.0$ μm). This dust partitioning is the same as that used by *Takemura et al.* [2000].

[16] One major challenge regarding the simulation of long-range transport of dust is how to calculate the dust emission rates. Mineral aerosols are emitted into the atmosphere as a result of high surface winds. In CFORS the total dust uplift flux, F_{dust} (kg/m^2/s), is calculated online using a power law function of surface friction velocity u_* [e.g., *Gillette and Passi*, 1988] as follows:

$$F_{dust} = C \cdot C_s \cdot C_W \cdot u_*^4 \left(1 - \frac{u_{*_{th}}}{u_*}\right) u_* > u_{*_{th}} \quad (3)$$

where the surface friction velocity u_* is transferred from the RAMS soil-vegetation scheme, u_{*th} is the threshold friction velocity for dust uplift, C is a dimensional constant equal to 7.5×10^5, C_s is the function of snow cover (set to zero for snow cover fraction >0.5), and C_w is a function of soil wetness.

[17] The threshold friction velocity u^*_{th} is important for controlling the dust emission and it is set as a function of soil texture. Global $1^\circ \times 1^\circ$ resolution soil texture data [*Zobler*, 1986] was used to identify the soil texture type in each grid. The empirical relationship between soil texture and roughness length, u^*_{th} based on the work by *Marticorena and Bergametti* [1995] and *Marticorena et al.* [1997] was used. The total dust uplift flux, F_{dust}, is subdivided into each size bin according to the initial dust-size distribution spectrum [*d'Almeida and Schutz*, 1983], which is unconditionally used in all of the dust emission regions. The initial dust uplift height (i.e., the injection height) is highly uncertain. In the CFORS dust module, the mixing height Z_{BL} is diagnosed from the vertical potential temperature profile (from RAMS), and the uplifted dust mass is uniformly distributed within the Z_{BL}.

[18] Identification of natural dust source regions is a key issue in the analysis of dust outbreaks. Within CFORS, the natural dust emission areas are defined as desert and semi-desert areas from the data set of 1-km resolution land cover characteristics produced by U.S. Geological Survey (USGS) (based on AVHRR data obtained in 1992/93). By using this method, large parts of the Gobi and Takla Makan Deserts are indexed as source regions. The Loess Plateau and the Nei Mongol's small desert (especially the north-west of Shenyang city, China) were further assigned as dust source areas on the basis of surface observations (SYNOP) dust reports and TOMS AI (aerosol index). Dust cannot be emitted from areas covered by snow. In CFORS monthly snow cover data was used to mask emission areas (e.g., many parts of the Himalayan mountain range), providing a seasonal element to dust emissions. Gravitational settling was accounted for using Stokes law ($\rho_{dust} = 2.52 \times 10^3$ kg/m^3) and the dust coagulation process was ignored. Dry deposition and wet scavenging parameters are shown in Table 2. Total dust emission flux based on the postanalysis of ACE-Asia is shown in Figure 3. More detailed dust emission schemes are available [e.g., *Nickovic et al.*, 2001; *Gong et al.*, 2003; *Zender et al.*, 2003] and they are now being evaluated within CFORS.

2.2.2. Anthropogenic Pollutants

[19] The anthropogenic emission inventories (SO_x, NO_x, CO, black carbon, organic carbon and hydrocarbons) were taken from the work of *Streets et al.* [2003]. These emissions were prepared specifically for TRACE-P and ACE-Asia experiments.

[20] The online tracers in CFORS can be chemically converted using linear processes. For example, the chemical reaction production of aerosol sulfate (SO_4) is assumed to be,

$$\frac{d[SO_4^{2-}]}{dt} = \frac{3}{2} \cdot k \cdot [SO_2] \quad (4)$$

where [X] is the mass mixing ratio of a substance X and k is the first-order chemical reaction rate constant (here k is set to 1.0%/h for SO_2 [*Carmichael et al.*, 2002]; it should be mentioned that the factor of 3/2 is necessary to convert Kg-SO_2/Kg-air to Kg-SO_4^{2-}/Kg-air). Table 2 shows the detailed parameters for each of the chemical tracers used in CFORS calculation.

[21] Anthropogenic BC and OC emissions were estimated for various sectors including industry, domestic (including combustion of biofuels, such as wood, crop residues, and dung), transport, and power generation. BC and OC emission from "open" burning (forest burning, savanna/grassland burning, and the burning of crop residues in the field after harvest) were estimated separately [*Streets et al.*, 2003]. The total anthropogenic BC and OC emissions in the CFORS domain (described later) between March and April 2001 are estimated to be 0.29 Tg and 1.34 Tg, respectively. It should be noted that the BC and OC emission inventory is highly uncertain as discussed by *Streets et al.* [2003]. The inventory has been assessed using CFORS/STEM analysis and there is a possibility of under estimation of emissions from the Chinese residential sector as reported by *Carmichael et al.* [2003a]. Furthermore, the emissions do not include the emission from Russia (including the biomass burning from there). In the analysis, black and organic carbon were assumed to exist solely in the fine mode and we ignored gravitational settling, wet deposition for BC, and chemical aging processes.

[22] One of the unique features of CFORS is the inclusion of the Megacity tracer. In Asia, there are several huge cities,

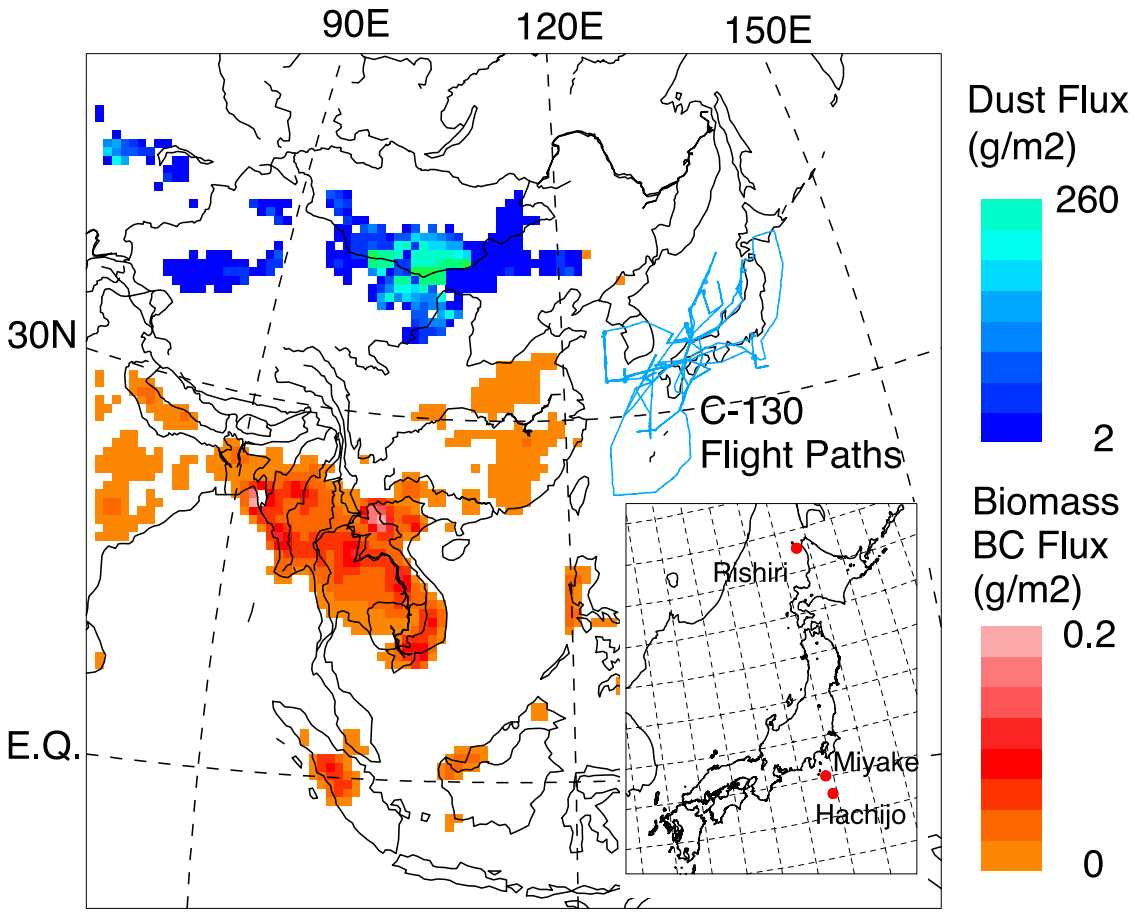

Figure 3. RAMS/CFORS model domain, C-130 flight paths (in blue line), dust emission flux and biomass black carbon emission flux between 1 March and 30 April 2001 used in the CFORS model simulations. Inset: Zoom-up map of Japan and VMAP observation sites, Rishiri and Hachijo.

such as Shanghai, Beijing, Hong Kong, Seoul and Tokyo, which we refer to as Megacities. CFORS releases an unreactive tracer (emission intensity is set proportional to the SO_2 emission rate) to identify the location of the megacity plumes. This feature was very useful in the design and analysis of the field experiments.

2.2.3. Biomass Burning BC, OC, and CO

[23] Another important aerosol gas/source in the springtime in Asia is associated with biomass burning. In CFORS separate tracers for CO, BC and OC from biomass burning sources are treated. Because biomass burning has important day-to-day variations due to local agricultural practices and precipitation amounts, daily emissions were estimated. Monthly emissions were calculated for each region on the basis of statistics of the types and amounts of biomass burned. These monthly amounts were then parsed into gridded daily emissions using AVHRR satellite fire counts [*Streets et al.*, 2003]. The total emissions of BC and OC from biomass burning within the CFORS domain were 0.17 Tg and 1.27 Tg, respectively. BC and OC emissions were distributed within the mixing height Z_{BL}. Distribution of modeled dust and biomass BC emissions during the postanalysis period are shown in Figure 3.

2.2.4. Sea Salt

[24] Sea salt can play an important role in radiative transfer. Sea salt emissions were calculated in 12 bins (0.005–20.5 μm radius) based on the work of *Gong et al.* [1997]. In the present study, CFORS only transported fine and coarse sea salt sizes; the 12 bins were summed into 2 bins (0.005–2.5 μm and larger than 2.5 μm) when transported within in CFORS.

2.2.5. Lighting NO_x

[25] Lighting NO_x is included as a tracer in CFORS to provide estimates of air masses impacted by lightning. Lightning NO_x emissions are calculated online on the basis of estimates of subgrid-scale cumulus activity calculated by a simplified Kuo cumulus scheme. Lightning NO_x emissions (function of cumulus cloud top) are distributed vertically between cloud base and cloud top as discussed by *Pickering et al.* [1998].

2.2.6. Volcanic SO_2

[26] Volcanoes are one of major sources of sulfur dioxide in Asia, and CFORS includes a volcano tracer. Estimated volcano SO_2 emissions for the major active volcanoes within the modeling domain were taken from *Fujita et al.* [1992]. The volcano on the Miyakejima island (Mt. Oyama; Longitude 139.55°E, Latitude 34.07°N and volcano height 818 m) south of Japan erupted in July 2000. An emissions rate of 10 million tons-SO_2/year (http://staff.aist.go.jp/kazahaya-k/SO2average.htm) is included in the CFORS for the Spring 2001 period. All the volcanic SO_2 emissions are injected into vertical layers between

1000–2000m. These emissions are included in the online calculations of total SO_2/Sulfate. CFORS also includes an unreactive volcano tracer to keep track of air masses impacted by volcanic emissions.

2.2.7. Radon

[27] Radon is a good tracer to identify the air masses of land origin. Radon emissions are specified following the approach of *Jacob et al.* [1997]. Radon (^{222}Radon) is assumed to be emitted only from land surfaces, with a constant emission rate of (1 molecule/cm^2/sec). This emission rate was modified by the land fraction of the model grid; over small isolated islands local radon emission were set to zero. No emissions were allowed to occur over areas covered by snow (snow coverage data is taken from monthly analysis). A half-life of 3.8 days was used, and depositions (dry and wash out) set to zero. The CFORS radon output comparison with the observations at Cheju (Korea) and Hok Tsui (Hong Kong) during the ACE-Asia observation period is reported by W. Zahorowski et al. (Atmospheric radon-222 at three ACE-Asia sites, submitted to *Journal of Geophysical Research,* 2003) (hereinafter referred to as Zahorowski et al., submitted manuscript, 2003).

2.3. Host Meteorological Analysis Data and CFORS Forecasting Operation

[28] RAMS is a regional meteorological model and requires initial and boundary meteorological conditions. For long-term simulations, a four-dimensional data analysis (FDDA) option using the nudging technique was included based on the RAMS (Isentropic Analysis Package (ISAN) output. RAMS/ISAN is designed to accept objective meteorological analysis data from various sources. ISAN converts the longitude-latitude grid with specified pressure coordinate data to the RAMS rotated polar stereographics terrain following vertical coordinate system. ISAN requires the horizontal wind components, temperature, geopotential height and relative humidity, so most of global/regional analysis data set from NCEP, JMA and ECMWF can be used in RAMS/ISAN. Here we refer to these global/regional analysis data sets as ''host meteorological data.'' RAMS/CFORS hindcast calculations were based on reanalysis data, while the forecast calculations were based on the operational weather forecasted ''host meteorological data'' sets, which were available from the NCEP and JMA.

[29] During the ACE-Asia and TRACE-P intensive observations, CFORS was run in an operational forecasting mode and provided daily forecasts of meteorology and gas/aerosol distributions. A unique element of the operational model was that two separate forecasts were produced each day; one where the RAMS model was initialized by NCEP (National Center for Environmental Prediction/NOAA; 96 hour forecasting AVN data set of $1^\circ \times 1^\circ$ degree resolution; http://www.emc.ncep.noaa.gov/modelinfo/index.html); and the second using Japan Meteorological Agency (JMA); 72 hour forecasting ASIA domain data set of $1.25^\circ \times 1.25^\circ$ degree resolution; (http://ddb.kishou.go.jp/) products. Data were downloaded from NCEP and JMA once per day. Sometimes the ''host meteorological data'' could not be downloaded because of internet traffic problems and/or computer system problems. The downloaded data sets were a combination of the analysis data (0UTC) and forecasting phase data (except for 0UTC). The JMA data set only covered up to 100hPa level in vertical dimension. We produced two separate forecasts each day using JMA and NCEP data in order to increase the forecast completeness (i.e., the ability to produce a forecast everyday), and to provide some appreciation/measure of uncertainty in the forecasts.

[30] The daily operational forecasting procedure is outlined in Figure 1. The system involves the use of three important servers: (1) CFORS ftp server accesses to the operational global forecast data set to NCEP and Asian forecast data set to JMA site. (2) CFORS main server calculates RAMS weather forecast for 72 hours on the basis of the NCEP and JMA data set as a lateral boundary condition. Chemical Transport Module integrating regional atmosphere and chemical transports. Pentium-III Linux cluster of 17 nodes are used for calculation. (3) CFORS web manager generates the post-processing of chemical weather forecast results with 2 & 3-D graphics into the CFORS web page. It used CGI interactive interface and can plot 2-D fields and time-height cross section at fixed points according to user's requests. It also has a switch for quick animation including vis5D 3-D views. Table 2 also lists the variables accessible from the web site. The current CFORS web site can be accessed at http://cfors.riam.kyushu-u.ac.jp/~cfors/index.html.

[31] Figure 3 shows the numerical model domain of CFORS during the TRACE-P/ACE-Asia operation, which is centered at 25°N 115°E on the rotated polar stereographics system. The horizontal grid consists of 100 by 90 grid points, with a resolution of 80 km. The model's vertical domain extends from surface to 23km with 22 stretching grid layers varying from 150 m thick at the surface to 1800 m thick at the top. Elevation of each grid center is 72, 236, 433, 670, 954, 1294, 1703, 2193, 2782, 3489, 4337, 5354, 6575, 8047, 9766, 11579, 13379, 15179, 16979, 18779, 20579, 22379 m. This model domain is able to simulate the important processes impacting chemical phenomena in East Asia.

[32] In the forecast model we used climatological monthly SST (sea surface temperature) and snow-cover data as the boundary conditions for the RAMS calculation. In addition, during the operational forecast period, the CFORS system was spun-up beginning 10 January 2001, and all the concentrations were initialized during the 2 months of continuous operation before the TRACE-P intensive operation. CFORS in forecast mode was restarted everyday by using the previous days history output file.

2.4. CFORS Postanalysis (Hindcast) During ACE-Asia

[33] In the postanalysis we utilized the ECMWF reanalysis data, with $1^\circ \times 1^\circ$ degree resolution (6 hour interval at specified pressure level of 1000, 925, 850, 700, 500, 400, 300, 250, 200, 150, 100, 70, 50, 30, 10 hPa). The ECMWF data set was used since it was provided with a higher spatial resolution than JMA. CFORS was applied in hindcast mode for the period 20 February 2001 through 31 May 2001. In the postanalysis study, we used analyzed weekly SST data, and observed monthly snow-cover data. The analysis of forecasting skill and variability between

JMA, NCEP and ECMWF fields are the subject of a future paper.

3. Results and Discussion

[34] CFORS was applied for the first time during the Spring 2001 TRACE-P and ACE-Asia experiments. Here we examine how well the CFORS results represent the observed variation of meteorological parameters and surface concentration fields at two Japanese island stations during the ACE-Asia intensive period. A detailed analysis of the performance of RAMS/CFORS based on the comparison from several observation platforms is presented elsewhere; for the TRACE-P experiment [*Carmichael et al.*, 2003a, 2003b], ACE-Asia heavy dust storm (J. H. Seinfeld et al., Regional climatic and atmospheric chemical effects of Asian dust and pollution, submitted to *Bulletin of the American Meteorological Society*, 2003, hereinafter referred to as Seinfeld et al., submitted manuscript, 2003), surface black carbon analysis [*Uno et al.*, 2003; *Matsumoto et al.*, 2003b], Mie scattering Lidar data analysis [*Sugimoto et al.*, 2002; *Shimizu et al.*, 2002], surface radon data analysis (Zahorowski et al., submitted manuscript, 2003), and monthly averaged aerosol fields.

3.1. Meteorological Fields

[35] Accurate characterization of the transport processes is of critical importance to flight planning and to the analysis of the observations. As shown in Figure 3, the NCAR C-130 aircraft flew 19 missions from 31 March to 4 May 2001 around Korea-Japan. Figure 4 shows the comparison between ACE-Asia C-130 observed meteorological parameters (wind speed, wind direction, air temperature and relative humidity) with RAMS/CFORS meteorological output. The model output was extracted along the C-130 aircraft observation points and compared to the 3-minute averaged observations. Air temperature, wind speed and wind direction show good agreement with C-130 measurements, while modeled relative humidity has a small wet bias under low relative humidity conditions. For example, correlation coefficients for all C-130 flights are: 0.89, 0.98, 0.98 and 0.83 for wind speed, temperature, pressure and relative humidity, respectively. These results show that CFORS is able to accurately capture many of the important observed meteorological features. It should be noted here that the results presented are from the hindcast analysis. However, the forecast and hindcast fields were quite similar to each other during this period.

3.2. VMAP Surface Observation Data Analysis

[36] During ACE-Asia the Variability of Maritime Aerosol Properties (VMAP) network was operated by *Matsumoto et al.* [2003a, 2003b]. VMAP provides important surface measurements of aerosol composition (elemental and organic carbon, major ions, trace metals and number concentration) and trace gases (SO_2, O_3, CO and radon) at 4 remote islands in Japan (Rishiri 45.12°N, 141.20°E; Sado 38.25°N, 138.40°E; Hachijo 33.15°N, 139.75°E and Chichijima 27.07°N, 142.22°E). VMAP provides an excellent data set to evaluate the performance of CFORS output and to demonstrate how the tracer and meteorological information contained in CFORS can be used to help interpret the observations.

[37] Two of the islands are shown in Figure 3; Rishiri and Hachijo islands (horizontal distance between these two island is approximately 1500 km, and they belong to different weather systems). Details of the measurement methods for aerosols and trace metals are described by *Matsumoto et al.* [2003a, 2003b].

[38] Measured values of EC, aerosol aluminum (Al), fine mode nss-SO_4, ^{222}Radon and CO at Rishiri and Hachijo Islands are presented by symbols in Figures 5 and 6, respectively. Note that all of the dates are Julian days and all times are Japan Standard Time (JST). No CO observations were made at Hachijo, and to facilitate comparison with CFORS calculated dust, the observed Al is converted to a dust concentrations by multiplying by a factor of 12.5 by assuming aluminum content for dust of 8 %. In these figures, the calculated radon and CO fields are scaled because, as discussed previously, CFORS does not specify inflow lateral boundary concentrations. To facilitate a direct comparison with observations, CO is scaled assuming a background concentration of 150ppb (which is the minimum value observed at Rishiri). Two different lines are shown for CO in Figure 5d; CO $\times$ 1 (dashed line) and CO $\times$ 2 (straight line). The twice concentration line is included because CFORS CO only represents a tracer for primary CO (i.e., chemically produced CO from hydrocarbon oxidation is not included). For radon, modeled radon is scaled by 4 $\times$ (CFORS-radon) + 3 [Bq] for Rishiri and 2 $\times$ (CFORS-radon) + 0.4 [Bq] for Hachijo (Bq represents the Radon concentration of becquerel/m^3). The background values are taken from the minimum values observed, and the difference in scaling factors may reflect limitations to the assumed uniform Radon emission rate and/or local radon emissions from islands (which were assumed to be zero).

[39] It is also important to note the differences in time resolution of the various observations. Al and nss-SO_4 represent daily averaged concentrations, EC is 4 hours averaged values, Radon and CO are 1 hour averaged values. The CFORS model values represent instantaneous 3 hour values. Details of radon observations are reported by K. Yoshioka (personal communication, 2002) and for CO by *Tanimoto et al.* [2000].

[40] Table 3 shows the statistical comparisons (mean, standard deviation, and coefficient of variation) between the observation and model results. We will discuss the detailed comparison in the following subsections.

3.2.1. Rishiri Surface Data Analysis

[41] Detailed observational data analysis is presented by *Matsumoto et al.* [2003b], so here we will focus on the use of CFORS output to help understand the time variation of gas/aerosols and air mass history observed at Rishiri. The CFORS predictions at Rishiri are shown in Figure 5. The averaged concentrations below z = 300 m are denoted by the line. In Figure 5a, the dashed line shows the modeled wind direction at 500 m level.

[42] At Rishiri, the time variation of CFORS tracers reproduces many of the observed variations. For example, Al is a good tracer of mineral dust, and observed Al concentrations at Rishiri increased on day 99 (9 April) as a result of a major dust storm that developed in China a few days earlier. Elevated levels of mineral dust associated with the dust outbreak arrived at Rishiri on day 99 (9 April), and elevated dust levels continued for three day. Dust emissions

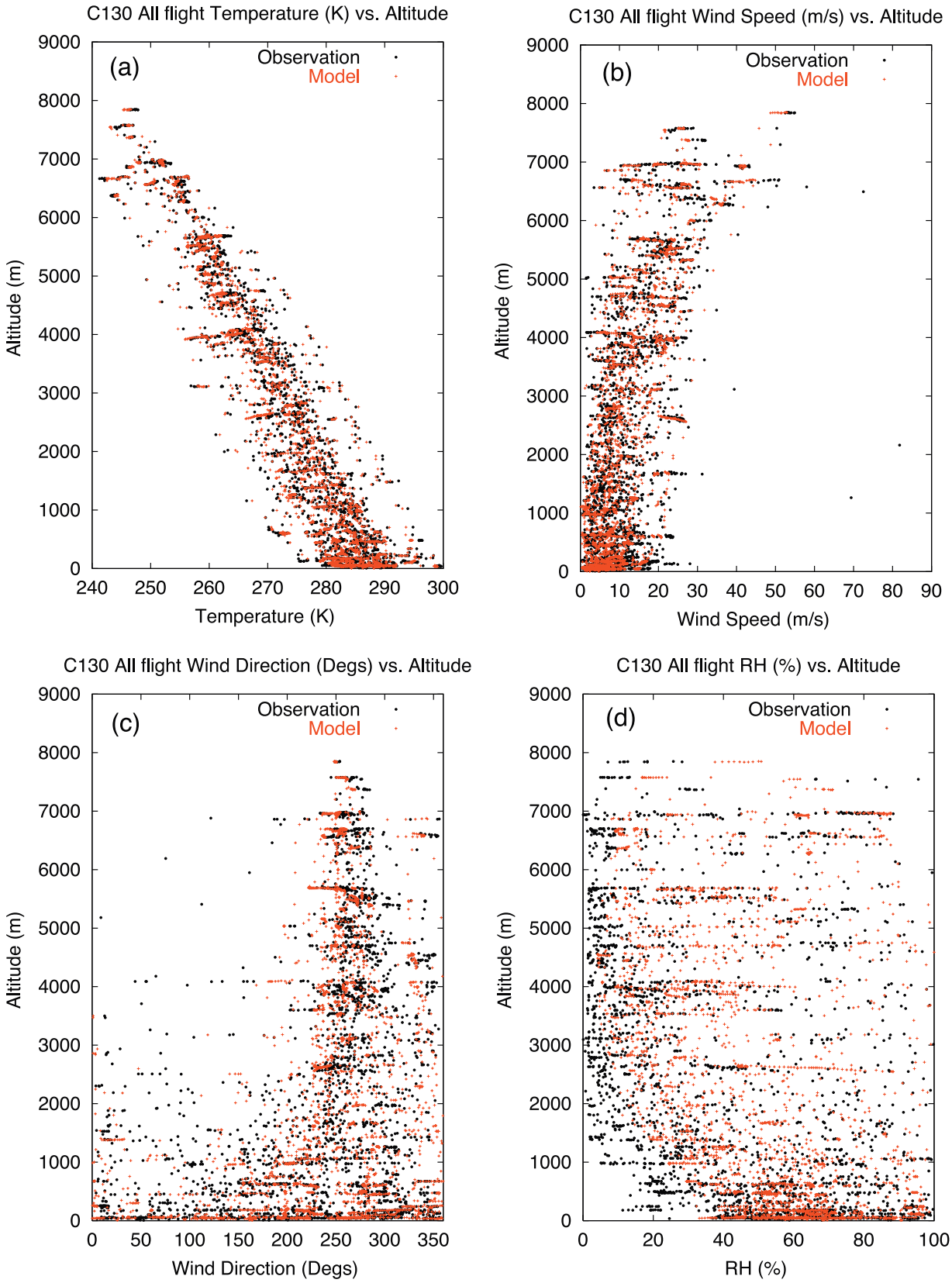

Figure 4. (a–d) Comparison between ACE-Asia C-130 airborne meteorological parameters and CFORS output fields along the flight tracks. (Aircraft C-130 flight parameters are taken from World Wide Web server for ACE-Asia: Asian Pacific Regional Aerosol Characterization Experiment at http://www.joss.ucar.edu/ace-asia/dm/data_access_frame.html.)

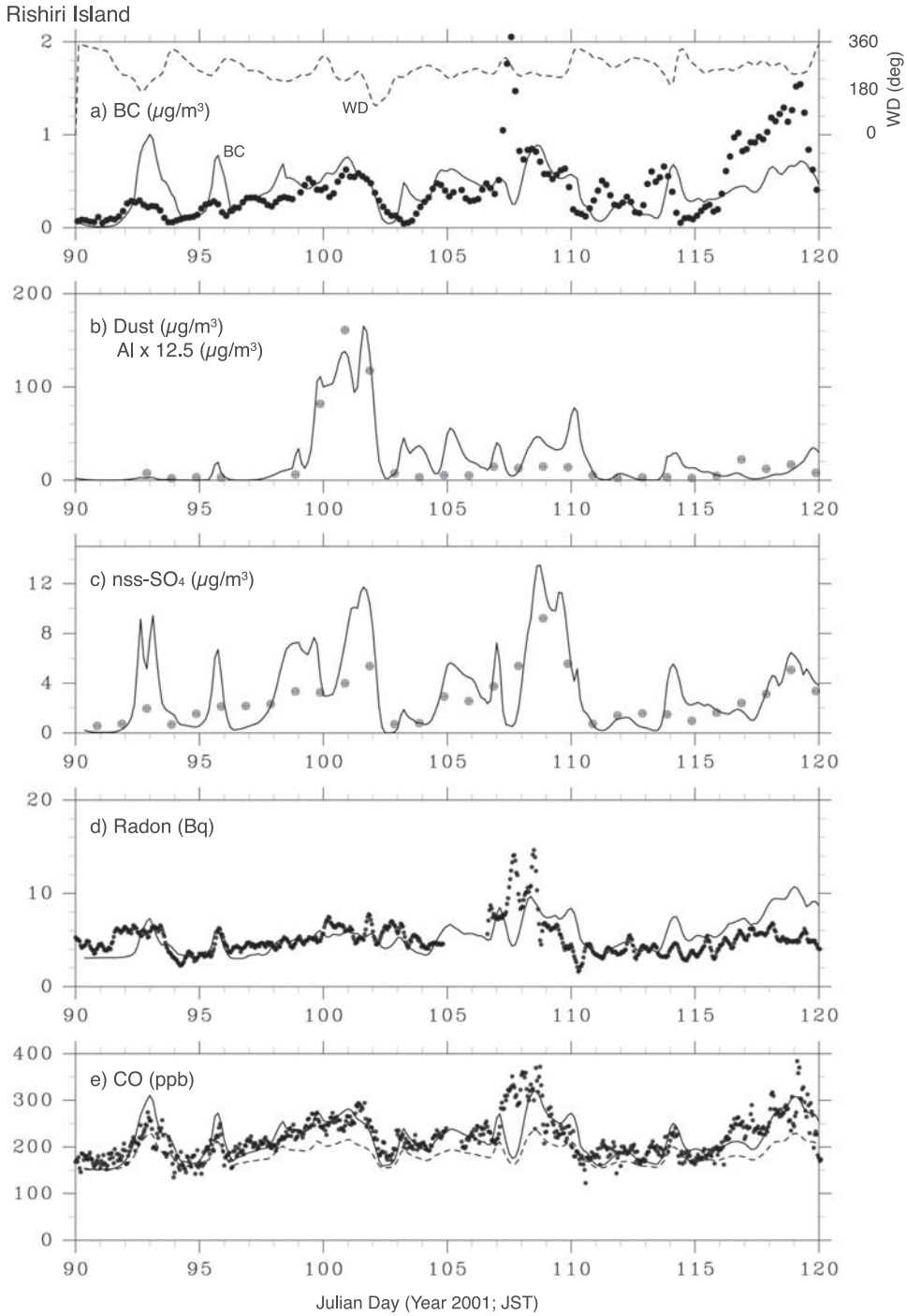

Figure 5. Comparison between observed concentrations at Rishiri island and CFORS model output (a) black carbon, (b) dust and Al, (c) nss-SO_4, (d) radon and (e) CO.

and dust outbreaks from the Asian continent occur sporadically. Depending on the height and pathway of the transport, dust may or may not exhibit a correlation with anthropogenic chemical components (such as SO_4, BC and CO). During the dust event on days 99 and 102, nss-SO_4 (days 100–102) had a strong correlation with BC and Al (dust). This indicates that anthropogenic pollutants such as BC and SO_4 were simultaneously transported along with the mineral dust. We can see that the model over predicted dust on days 105 and 110. One reason for this over prediction can be explained by the vertical dust profile shown in Figure 7. On days 105 and 110, the model simulated elevated dust layers; too strong vertical mixing processes (transportation from elevated dust layer to the surface) in the model at this time could be a reason for this discrepancy.

[43] In the case of sulfate, the model has a tendency to over predict before day 102 (but notice that the gradual increasing trend from day 97 to 101 is reproduced). This over prediction can also be seen in BC for days 92–93 and 95–96. On these days, RAMS predicted significant precipitation, and modeled wet removal for BC and SO_4 may be too weak during this event. It is also important to note that

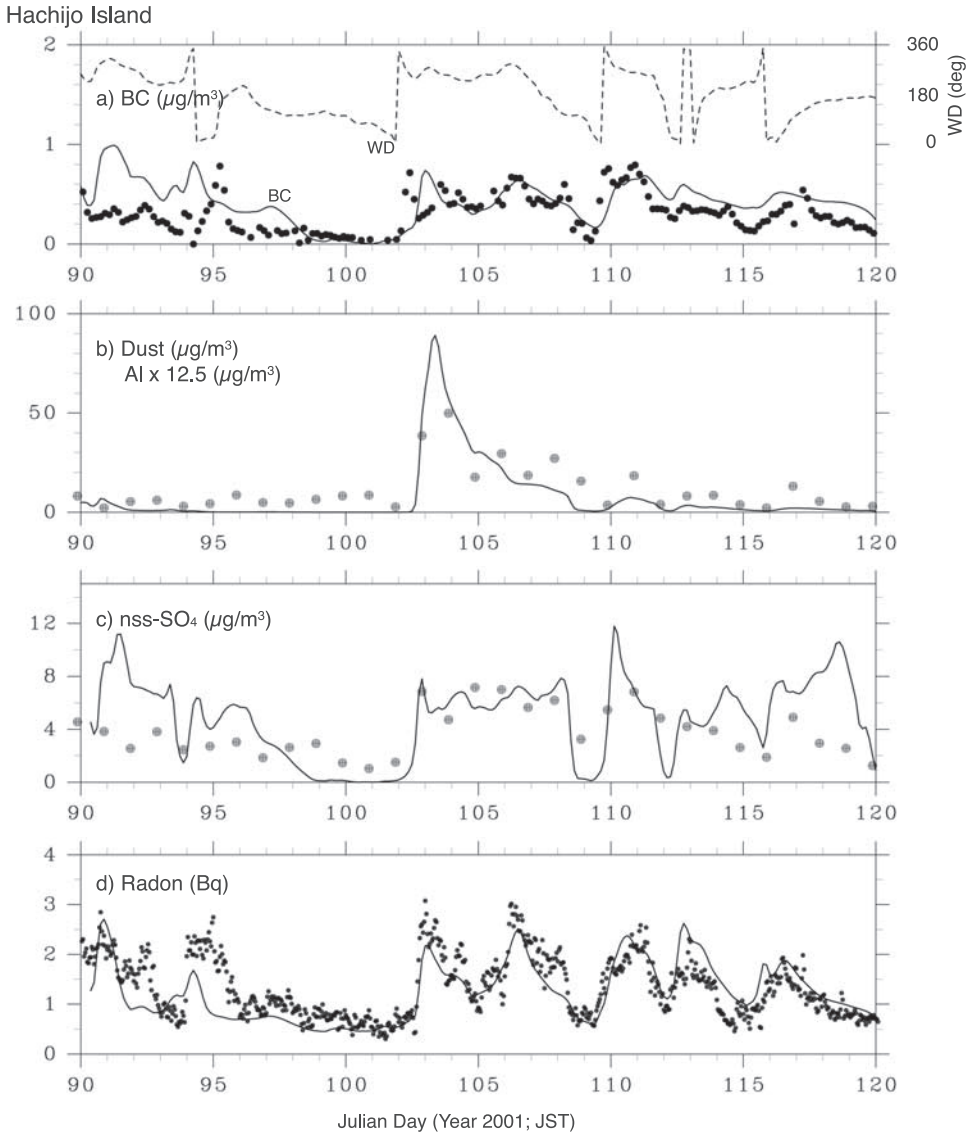

Figure 6. Comparison between observed concentrations at Hachijo island and CFORS model output. (a) black carbon, (b) dust and Al, (c) nss-SO_4 and (d) radon.

large horizontal gradients of SO_4 are predicted around the latitude of 40–45°N. Under such a situation, slight changes in the timing and/or spatial location of the transport pathways (e.g., errors in modeled meteorology) can lead to large variations in the time series at a fixed point. Sulfate concentrations are simulated well after day 102.

[44] A peak in BC, Radon and CO is observed on day 107 (17 April), which is not captured in the model. Observed SO_4 does not show this peak. Model simulated horizontal SO_4 distribution is shown in Figure 8f. We can see that a clean air mass existed to the west of Rishiri. *Matsumoto et al.* [2003b] discussed this EC peak on the basis of optical particle counter (OPC) and other chemical tracers and indicated the possibility of biomass or forest fire influences from the far east Russia. Further study is needed to identify the origin of this plume.

[45] The CFORS scaled radon and CO show good agreement with the observations. As listed in Table 3, the standard deviation and coefficient of variation (C.V.) are

Table 3. Statistical Comparisons of Model and Observations[a]

	Observations			CFORS		
Tracers	Mean	s.d.	C.V.	Mean	s.d.	C.V.
			Rishiri			
Radon, Bq/m^3	4.88	1.20	0.25	5.42	1.47	0.27
EC (BC), μg/m^3	0.43	0.26	0.60	0.41	0.19	0.46
SO_4, μg/m^3	2.52	1.37	0.54	3.34	2.11[b]	0.63
Al (Dust),[c] μg/m^3	1.41	1.59	1.13	21.3	19.7[b]	0.92
CO, ppb	209.6	36.9	0.18	217.9[d]	35.6[d]	0.16
			Hachijo			
Radon, Bq/m^3	1.23	0.52	0.42	1.23	0.48	0.39
EC (BC), μg/m^3	0.33	0.15	0.45	0.40	0.16	0.40
SO_4, μg/m^3	3.70	1.51	0.41	4.82	2.20[b]	0.46
Al (Dust),[c] μg/m^3	0.83	0.63	0.75	22.9	24.9[b]	1.08

[a]Here, s.d., standard deviation; C.V., coefficient of variation.
[b]Evaluated by daily averaged value.
[c]Al is taken for observation and total dust concentration for model.
[d]Calculated by (CO − CFORS) × 2.

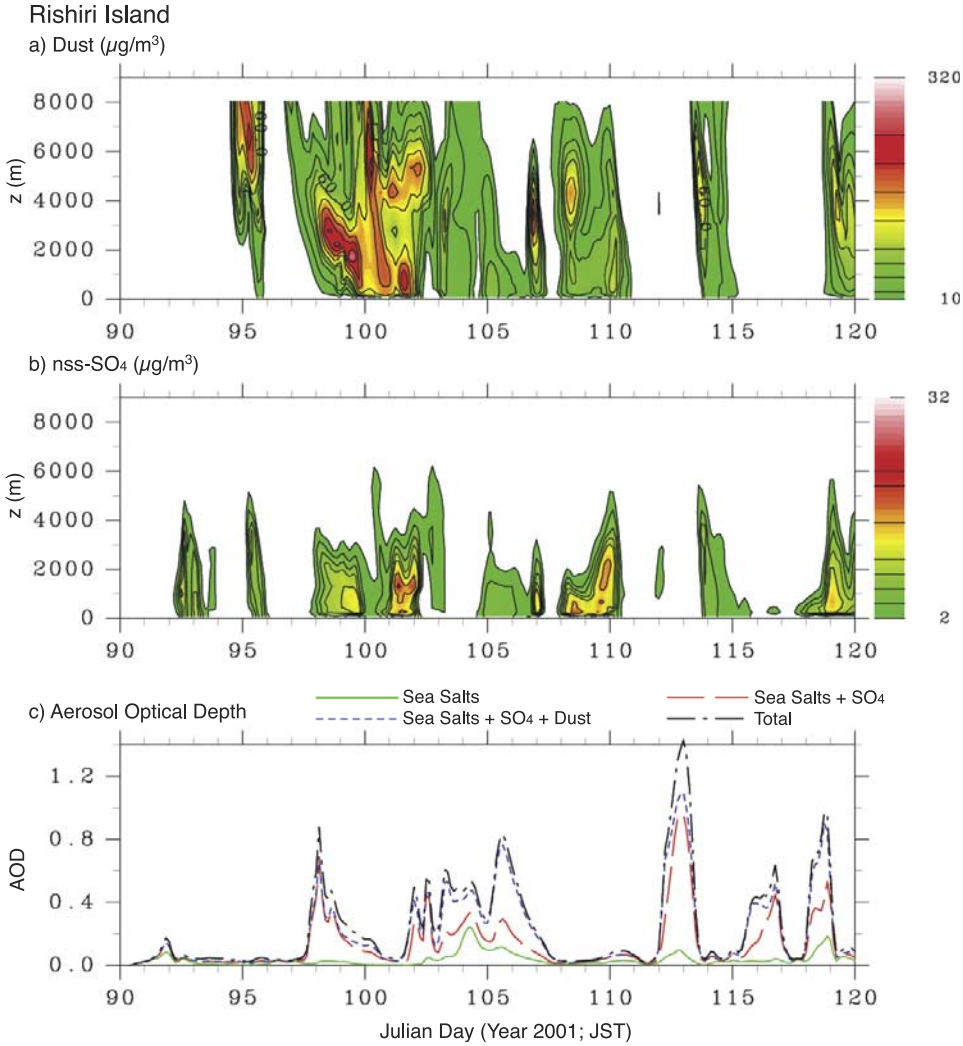

Figure 7. Time-height cross section of (a) mineral dust and (b) nss-SO_4. (c) Time variation of AOD (composite of aerosol categories) for Rishiri Island.

within ±10 % for CO and radon. This suggests that the CFORS model has skill in capturing the transport, removal, and large-scale emission processes that lead to variability in these tracers. However, the fact that the comparison uses scaled modeled tracers means that the emissions themselves cannot be evaluated from such comparisons.

[46] The correlation between the chemical tracers is also of interest and can provide additional information. *Matsumoto et al.* [2003b] found the regressions in the observations to be

$$[\mathrm{CO(ppb)}] = 126.9[\mathrm{EC}(\mu g/m^3)] + 159.0$$

$$[\mathrm{EC}(\mu g/m^3)] = 0.11\left[\mathrm{nss} - \mathrm{SO_4^{2-}}(\mu g/m^3)\right] + 0.07$$

The CFORS results are as follows:

$$[\mathrm{CO} - \mathrm{CFORS(ppb)}] = 131.7\left[\mathrm{BS} - \mathrm{CFORS}(\mu g/m^3)\right] + 165.6 \quad (R = 0.73)$$

$$\left[\mathrm{BC} - \mathrm{CFORS}(\mu g/m^3)\right] = 0.065\left[\mathrm{SO_4} - \mathrm{CFORS}(\mu g/m^3)\right] + 0.18 \quad (R = 0.82)$$

The CFORS results reproduced the observed correlation between CO and EC (BC) very well in terms of slope, intercept and correlation. For BC-CFORS and SO_4-CFORS, the slope is low, but is strongly influenced by the observed peak on days 107 and 117.

3.2.2. Hachijo Surface Data Analysis

[47] As shown in Figure 6, a polluted air mass was observed on day 102 (12 April) at Hachijo. BC, nss-SO_4 and radon concentrations showed a rapid increase on this day. CFORS captured these variations correctly. CFORS also predicted peak dust concentrations during days 102–103 (12–13 April; see Figures 6 and 8), which occurred several hours behind the arrival of the anthropogenic pollutants (see Figures 6b and 6c). Notice that observed nss-SO_4 and Al are daily averaged values, so we cannot see the time delay from the observation, but such a detailed time delay between dust and SO_4 was clearly reported by *Uematsu et al.* [2002].

[48] It is important to note that CFORS captures the onset of dust correctly, but that dust concentrations are over predicted. Quantitative prediction of dust remains difficult because of complexities in accurately calculating dust emissions.

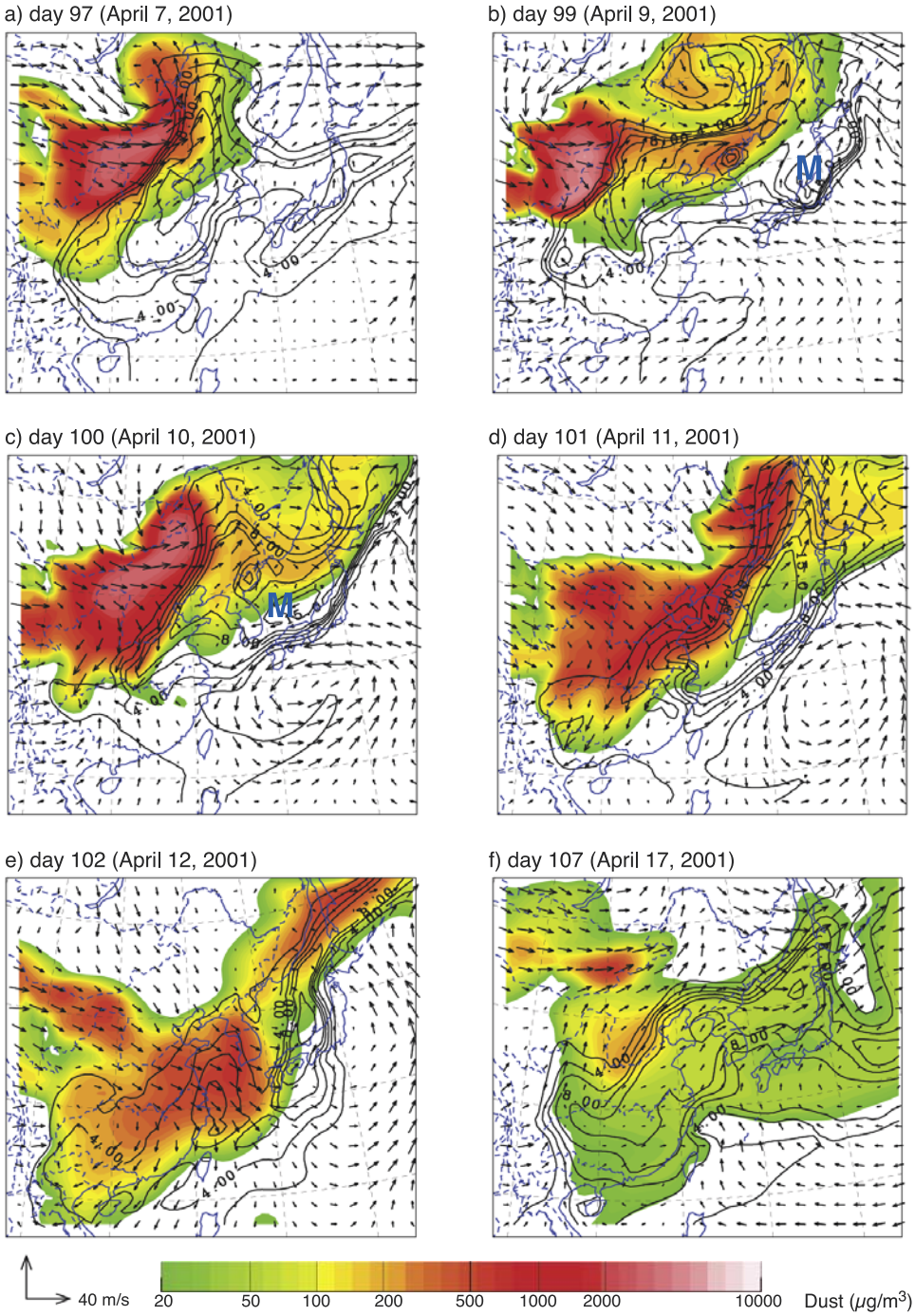

Figure 8. CFORS model output for boundary layer dust (color in log scale) and SO_4 (contour lines for 2,4,6,8,10,15 and 20 $\mu g/m^3$) concentration (surface - 1000m) and wind vector at 1000m. (a) day 97 (7 April), (b) day 99 (9 April), (c) day 100 (10 April), (d) day 101 (11 April), (e) day 102 (12 April), and (f) day 107 (17 April).

[49] SO_4 shows over prediction on days 92–93, 94–96 and 117–119. This fact can be understood by the emissions from the Miyakejima volcano. As described in section 2.2.6, the horizontal distance between Miyakejima and Hachijo is approximately 150 km, so the CFORS horizontal grid size of 80 km is too large and too often places the influence of Miyakajima into the Hachijo grid cell. Finer resolution calculations are needed to more accurately assess the role of Miyakajima emissions on Hachijo.

[50] As shown in Figures 8b–8d, the persistent east wind during the days 99–101 covered Hachijo because of the clockwise wind flow into the traveling cyclone. During this period, very clean maritime air mass from the Pacific Ocean was brought to Hachijo, and the chemical tracer concentrations were low (near the lower limit of detection).

[51] Radon is an excellent tracer to identify the air mass origin (continental air mass tracer) and both observations and model simulations indicate that radon and CO have a

strong correlation (see Figures 5c and 5d). The CFORS radon field captures the synoptic features at both of these islands sites. *Matsumoto et al.* [2003a] reported the correlation between radon and EC, and the regression lines averaged over April and May are

$$\left[\text{Radon}\left(\text{Bq/m}^3\right)\right] = 2.15\left[\text{EC}\left(\mu\text{g/m}^3\right)\right] + 0.77 \quad (\text{R} = 0.61) \text{ for Hachijo}$$

$$\left[\text{Radon}\left(\text{Bq/m}^3\right)\right] = 3.00\left[\text{EC}\left(\mu\text{g/m}^3\right)\right] + 4.08 \quad (\text{R} = 0.53) \text{ for Rishiri}$$

and CFORS results give

$$\left[\text{Radon}\left(\text{Bq/m}^3\right)\right] = 2.06\left[\text{EC}\left(\mu\text{g/m}^3\right)\right] + 0.39 \quad (\text{R} = 0.75) \text{ for Hachijo}$$

$$\left[\text{Radon}\left(\text{Bq/m}^3\right)\right] = 6.97\left[\text{EC}\left(\mu\text{g/m}^3\right)\right] + 3.09 \quad (\text{R} = 0.68) \text{ for Rishiri}$$

CFORS reproduces the relationship between Radon and EC very well for Hachijo, including the slope and correlation coefficient. The modeled slope at Rishiri is steeper than the observation, and this is most likely due to uncertainties in the assumed emission rate. SO_4 and Radon are also highly correlated at Hachijo because this island is located south of Japan main island, and continental air masses (characterized by anthropogenic emission) frequently pass over Japan before arriving to Hachijo.

3.3. Horizontal Distribution of Dust and Sulfate in April 2001

[52] CFORS results can also help in the interpretation of the surface observations by providing information about the horizontal and vertical distribution of pollutants. Figure 8 shows the horizontal distribution of dust (color) and sulfate(lines). During this period a major dust storm occurred that consisted of two major outbreaks of dust, which were viewed in Sea WIFS and TOMS AI images. The first occurred over the Gobi desert area (near the China and Mongolia boarder) on the day 95–96 (not shown, but Figure 8a is the results of this dust transport). This dust was transported at high latitudes (~40°N) and arrived at Rishiri on day 99–100. Dust from this event did not impact Hachijo. A second dust outbreak occurred on day 98–99 (Figure 8b). Dust from this event divided into two major air masses, one transported to Rishiri on the day 101, the second transported at lower latitudes, reaching Hachijo on day 102–103. These features are clearly seen in the VMAP surface observations (see Figures 5 and 6).

[53] It is important to point out that the main body of sulfate air mass (high-concentration region) and that of dust air mass are clearly separated; the main body of sulfate air mass is located mainly to the east of the dust. The typical example can be seen in Figures 8a–8d. We can see the steep sulfate gradient at the boarder between sulfate and dust (however we can also see the small mixing of dust and sulfate beyond the steep gradient zone). The large-scale dust onset is located behind the cold mesofront (see Figures 8a–8c), and the sulfate air mass is located in the warm sector. However, the clear separation of dust and sulfate cannot be seen on day 102. On this day, dust and sulfate are mixed over the East China sea and on the west-side of the Japan main island.

[54] We can see the high-sulfate air mass over the Japan sea on the days 99 and 100 (see marked as M in Figures 8b and 8c). A cold front was located northwest of Beijing on the day 99, and a large traveling low-pressure system was moving to the east from the north-east of Taiwan to the south of Tokyo (toward Hachijo). The counter-clockwise easterly winds brought relatively clean Pacific air and the volcano plume from Miyakejima to the central part of the Japan sea.

3.4. Time-Height Concentration Profile and Aerosol Optical Depth

[55] Examination of time-height concentration (TH plot) is another important usage of CFORS results. Some of important comparisons between observation and model are already reported by Seinfeld et al. (submitted manuscript, 2003) for ship borne measurements, and by *Shimizu et al.* [2002] and *Sugimoto et al.* [2002] for Mie Lidar measurements. At Rishiri and Hachijo, there were no vertical profiling observation data, however the examination of TH plot is important for understanding the surface measurement data. Here we will discuss the TH plots at Rishiri and Hachijo.

[56] The vertical distributions shown in Figures 7 and 9 reveal a complex layer structure in dust and SO_4. For example, the surface observations at Rishiri showed that on day 99 (9 April) elevated sulfate concentrations preceded the arrival of dust at the surface. The vertical plots show a layer of dust above the sulfate layer. This elevated dust layer descended to the surface on days 100 and 101 (10 and 11 April). Dust associated with the second dust outbreak was transported together with the sulfate as shown on day 102 (12 April). Elevated layers of dust are a common feature at Rishiri as shown on day 103, 107 and 109 (13, 17, and 19 April). The major storm tracks move off of Asia and pass over Rishiri, and dust lifted by these cold fronts are typically found at altitudes between 2 and 6 km.

[57] In contrast, dust is transported to Hachijo in descending air masses associated with high-pressure systems that follow the passages of the cold fronts. Here dust typically resides in the boundary layer along with other pollutants such as sulfate. However elevated sulfate layers are shown at Hachijo on days 96, 98, and 102–103 (6, 8, and 12–13 April). These are associated with the Mt. Oyama volcano (Miyakejima Island). Sulfate of volcanic origin is shown to be layered above the anthropogenic component. The carbonaceous aerosol has a unique structure at Hachijo, with elevated layers at 2–6 km (not shown). These layers represent air masses impacted by biomass burning in SE Asia and which have undergone long-distance transport in the warm conveyor belt associated with the frontal systems. In contrast, the boundary-layer carbonaceous aerosol has strong correlation with sulfate. This implies that BC in the boundary layer at Hachijo is influenced by nearby anthropogenic sources and is associated with the low-altitude outflow.

[58] The vertical structure helps to explain the AOD (aerosol optical depth) time-series shown in Figures 7 and 9.

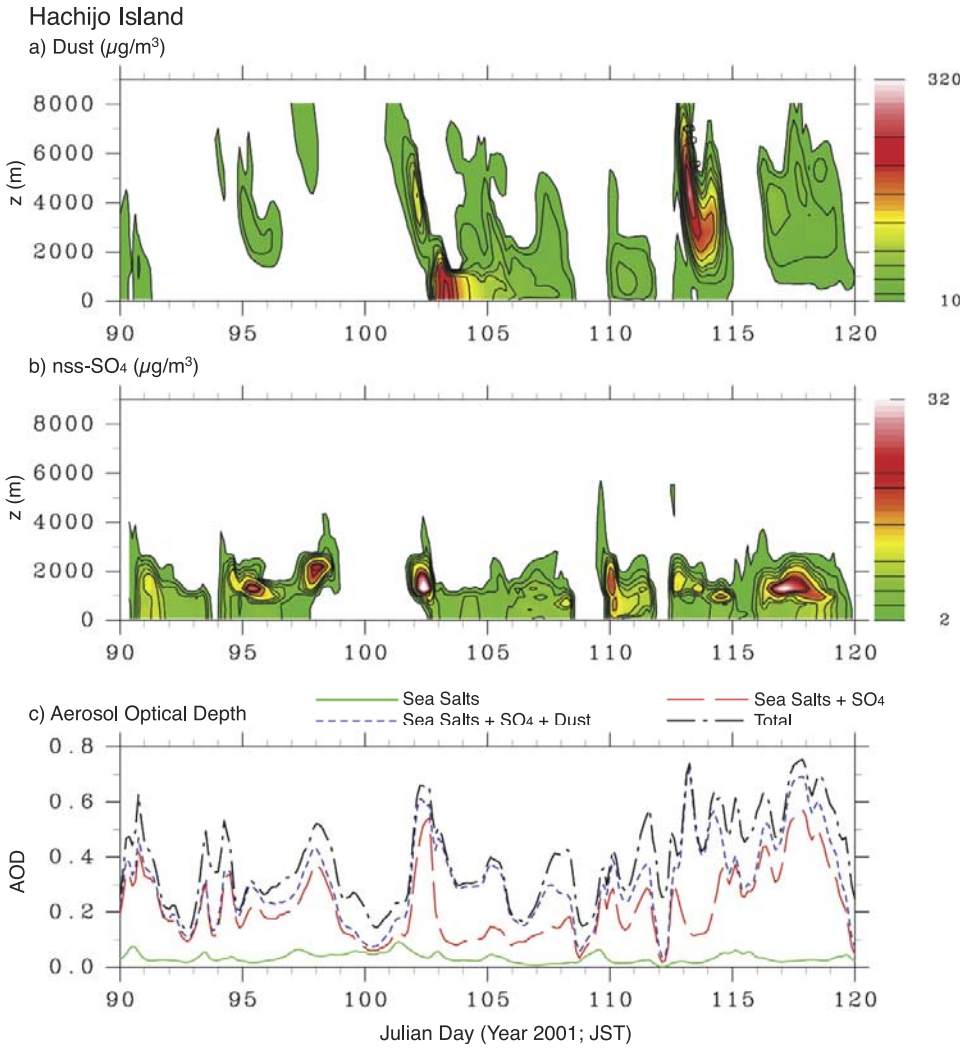

Figure 9. Time-height cross section of (a) mineral dust and (b) nss-SO_4. (c) Time variation of AOD (composite of aerosol categories) for Hachijo Island.

As shown there are significant differences between Rishiri and Hachijo islands. At Rishiri the mineral dust contribution to AOD is higher than that at Hachijo. In contrast, at Hachijo the carbonaceous fraction of AOD is more important. It is important to point out that Hachijo also has a large contribution to AOD from the elevated SO_4 layers arising from the volcano (Miyakejima Island). The sharp peaks both in surface SO_4 concentration and elevated SO_4 at day 102 (12 April) at Hachijo are associated with emissions from this volcano.

4. Concluding Remarks

[59] In this paper we presented the details of the chemical transport model Chemical Weather Forecast System (CFORS), a tool developed to assist in the design and interpretation of field experiments. CFORS was designed as a multitracer, online, system built within the Regional Atmospheric Modeling System (RAMS) [*Pielke et al.*, 1992]. A unique feature of CFORS is that multiple tracers are run online in RAMS, so that all the meteorological information from RAMS is directly used by the tracer model at every time step (~90 sec). As a result, CFORS produces with high-time-resolution 3-dimensional fields of tracer distributions and major meteorological parameters. During TRACE-P, ACE-Asia and ITCT-2K2 experiments a variety of tracers were used to help identify air masses from different sources (e.g., volcanoes, biomass burning, megacities).

[60] We also presented an evaluation/illustration of the performance of CFORS and how it can be used to help understand observational data. Specifically we presented results for VMAP surface sites. We showed that the CFORS model was able to capture many of the key details in the spatial and temporal distributions of the observations of CO, sulfate radon and mineral dust. CFORS meteorological fields (RAMS) also showed good agreement with ACE-Asia C-130 airborne meteorological observations, demonstrating that CFORS was able to reproduce the regional-scale meteorological variations over the different weather systems encountered during the experiments. Time-height cross-section analysis at Rishiri and Hachijo islands identified a complex layered structure in sulfate, dust, and carbonaceous aerosol associated with the frontal outflow. These results help explain the time variation of mineral aerosol observed during the ACE-Asia period, and also point out the need to complement surface measurements

with measurements above the surface (e.g., lidar and/or aircraft). We also identified circumstances where the model did not perform well. Important examples include overprediction of dust amounts and sulfate levels during periods at Hachijo. These point out the need to continue to improve the dust emissions algorithm in CFORS, and the important role that model resolution can play.

[61] We are now in the process of repeating the postanalysis using CFORS with a much finer resolution (~15 km). We are also developing a nested grid version of CFORS to provide a more flexible modeling tool. Furthermore, the results from CFORS are being used in the analysis of many different data sets obtained during the ACE-Asia, ITCT-2K2 and TRACE-P, and are the subject of several separate papers. The lessons learned from these studies will provide important guidance into how to improve CFORS.

[62] **Acknowledgments.** This work was partly supported by Research and Development Applying Advanced Computational Science and Technology (ACT-JST) and Core Research for Evolution Science and Technology (CREST) of Japan Science and Technology Corporation (JST). This work was also supported in part by grants from the NSF Atmospheric Chemistry Program, NASA ACMAP and GTE programs, and NOAA Global Change program. The authors want to express their thanks to Koji Ishihara for his great help in constructing the full automatic operational CFORS system during the field campaign and two anonymous reviewers for their valuable comments, which improved this paper.

References

Carmichael, G. R., L. K. Peters, and T. Kitada, A second generation model for regional-scale transport/chemistry/deposition, *Atmos. Environ.*, *20*, 173–188, 1987.

Carmichael, G. R., et al., The MICS-Asia study: Model intercomparison of long range transport and sulfur deposition in east Asia, *Atmos. Environ.*, *36*, 175–199, 2002.

Carmichael, G. R., et al., Evaluating regional emission estimates using the TRACE-P observations, *J. Geophys. Res.*, *108*, doi:10.1029/2002JD003116, in press, 2003a.

Carmichael, G. R., et al., Regional-scale chemical transport modeling in support of the analysis of observations obtained during the TRACE-P experiment, *J. Geophys. Res.*, *108*(D21), 8823, doi:10.1029/2002JD003117, in press, 2003b.

Chen, C., and W. R. Cotton, A one-dimensional simulation of the stratocumulus-capped mixed layer, *Boundary Layer Meteorol.*, *25*, 289–321, 1983.

Ching, J., and D. Byun (Eds.), Science algorithms of the EPA Models-3 community multi-scale air quality (CMAQ) modeling system, *Rep. EPA/600/R-99/030*, Natl. Exposure Res. Lab., Research Triangle Park, N.C., 1999.

d'Almeida, G. A., and L. Schutz, Number, mass and volume distributions of mineral aerosol and soils of the Sahara, *J. Clim. Appl. Meteorol.*, *22*, 233–243, 1983.

Ehhalt, D. H., F. Rohrer, A. B. Kraus, M. J. Prather, D. R. Blake, and F. S. Rowland, On the significance of regional trace gas distributions as derived from aircraft campaigns in PEM-West A and B, *J. Geophys. Res.*, *102*, 28,333–28,351, 1997.

Flatoy, F., O. Hov, and H. Schlager, Chemical forecasts used for measurement flight planning during POLINAT 2, *Geophys. Res. Lett.*, *27*, 951–954, 2000.

Fujita, S., Y. Tonooka, and K. Ohta, Annual contribution of volcanic sulfur dioxide emissions to the atmosphere in Japan, *J. Jpn. Soc. Air Pollut.*, *27*, 336–343, 1992.

Gillette, D., and R. Passi, Modeling dust emission caused by wind erosion, *J. Geophys. Res.*, *93*, 14,233–14,242, 1988.

Gong, S. L., L. A. Barrie, and J.-P. Blanchet, Modeling sea-salt aerosols in the atmosphere: 1. Model development, *J. Geophys. Res.*, *102*, 3805–3818, 1997.

Gong, S. L., X. Y. Zhang, T. L. Zhao, I. G. McKendry, D. A. Jaffe, and N. M. Lu, Characterization of soil dust aerosol in China and its transport and distribution during 2001 ACE-Asia: 2. Model simulation and validation, *J. Geophys. Res.*, *108*(D9), 4262, doi:10.1029/2002JD002633, 2003.

Huebert, B., T. Bates, P. Russell, G. Shi, Y. J. Kim, K. Kawamura, G. R. Carmichael, and T. Nakajima, An overview of ACE-Asia: Strategies for quantifying the relationships between Asian aerosols and their climatic impacts, *J. Geophys. Res.*, *108*(D23), 8633, doi:10.1029/2003JD003550, in press, 2003.

Jacob, D. J., et al., Evaluation and intercomparison of global atmospheric transport models using ^{222}Rn and other short-lived tracers, *J. Geophys. Res.*, *102*, 5953–5970, 1997.

Jacob, D. J., J. H. Crawford, M. M. Kleb, V. S. Connors, R. J. Bendura, J. L. Raper, G. W. Sachse, J. C. Gille, L. Emmons, and C. L. Heald, The Transport and Chemical Evolution over the Pacific (TRACE-P) aircraft mission: Design, execution, and first results, *J. Geophys. Res.*, *108*(D20), 8781, doi:10.1029/2002JD003276, in press, 2003.

Lawrence, M. G., Evaluating trace gas sampling strategies with assistance from a global 3D photochemical model: Case studies for CEPEX and NARE O3 profiles, *Tellus, Ser. B*, *53*, 22–39, 2001.

Lawrence, M. G., et al., Global chemical weather forecasts for field campaign planning: Predictions and observations of large-scale features during MINOS, CONTRACE, and INDOEX, *Atmos. Chem. Phys.*, *3*, 267–289, 2003.

Lee, A. M., G. D. Carver, M. P. Chipperfield, and J. A. Pyle, Three-dimensional chemical forecasting: A methodology, *J. Geophys. Res.*, *102*, 3905–3919, 1997.

Lee, T. J., The impact of vegetation on the atmospheric boundary layer and convective storms, *Atmos. Sci. Pap. 509*, Dep. of Atmos. Sci., Colo. State Univ., Fort Collins, 1992.

Louis, J.-F., A parametric model of vertical eddy fluxes in the atmosphere, *Boundary Layer Meteorol.*, *17*, 187–202, 1979.

Marticorena, B., and G. Bergametti, Modeling the atmospheric dust cycle: 1. Design of a soil-derived dust emission scheme, *J. Geophys. Res.*, *100*, 16,415–16,430, 1995.

Marticorena, B., G. Bergametti, D. Gillette, and J. Belnap, Factors controlling threshold friction velocity in semiarid and arid areas of the United States, *J. Geophys. Res.*, *102*, 23,277–23,287, 1997.

Matsumoto, K., M. Uematsu, T. Hayano, K. Yoshioka, H. Tanimoto, and T. Iida, Simultaneous measurements of particulate elemental carbon on the ground observation network over the western North Pacific during the ACE-Asia campaign, *J. Geophys. Res.*, *108*(D23), 8635, doi:10.1029/2002JD002744, in press, 2003a.

Matsumoto, K., Y. Uyama, T. Hayano, H. Tanimoto, I. Uno, and M. Uematsu, Chemical properties and outflow patterns of anthropogenic and dust particles on Rishiri Island during the Asian Pacific Regional Aerosol Characterization Experiment (ACE-Asia), *J. Geophys. Res.*, *108*(D23), 8666, doi:10.1029/2003JD003426, in press, 2003b.

Mellor, G. L., and T. Yamada, A hierarchy of turbulence closure models for planetary boundary layers, *J. Atmos. Sci.*, *31*, 1791–1806, 1974.

Mellor, G. L., and T. Yamada, Development of a turbulent closure model for geophysical fluid problems, *Rev. Geophys.*, *20*, 851–875, 1982.

Nickovic, S., G. Kallos, A. Papadopoulos, and O. Kakaliagou, A model for prediction of desert dust cycle in the atmosphere, *J. Geophys. Res.*, *106*, 18,113–18,129, 2001.

Pickering, K. E., Y. Wang, W.-K. Tao, C. Price, and J.-F. Müller, Vertical distributions of lightning NO_x for use in regional and global chemical transport models, *J. Geophys. Res.*, *103*, 31,203–31,216, 1998.

Pielke, R. A., et al., A comprehensive meteorological modeling system - RAMS, *Meteorol. Atmos. Phys.*, *49*, 69–91, 1992.

Shimizu, A., N. Sugimoto, I. Matsui, K. Arao, T. Murayama, N. Kagawa, and I. Uno, Continuous observations of Asian dust and other aerosols by dual-polarization lidars in China and Japan during ACE-Asia, *J. Geophys. Res.*, *108*, doi:10.1029/2002JD003253, in press, 2002.

Streets, D. G., et al., An inventory of gaseous and primary aerosol emissions in Asia in the year 2000, *J. Geophys. Res.*, *108*(D21), 8809, doi:10.1029/2002JD003093, in press, 2003.

Sugimoto, N., I. Matsui, A. Shimizu, I. Uno, K. Asai, T. Endoh, and T. Nakajima, Observation of dust and anthropogenic aerosol plumes in the northwest Pacific with a two-wavelength polarization lidar on board the research vessel *Mirai*, *Geophys. Res. Lett.*, *29*(19), 1901, doi:10.1029/2002GL015112, 2002.

Takemura, T., H. Okamoto, Y. Maruyama, A. Numaguti, A. Higurashi, and T. Nakajima, Global three-dimensional simulation of aerosol optical thickness distribution of various origins, *J. Geophys. Res.*, *105*, 17,853–17,873, 2000.

Tanimoto, H., Y. Kajii, J. Hirokawa, H. Akimoto, and N. P. Minko, The atmospheric impact of boreal forest fires in far eastern Siberia on the seasonal variation of carbon monoxide: Observations at Rishiri, a northern remote island in Japan, *Geophys. Res. Lett.*, *27*, 4073–4076, 2000.

Tremback, C. J., Numerical simulation of a mesoscale convective complex: Model development and numerical results, *Atmos. Sci. Pap. 465*, Dep. of Atmos. Sci., Colo. State Univ., Fort Collins, 1990.

Uematsu, M., A. Yoshikawa, H. Muraki, K. Arao, and I. Uno, Transport of mineral and anthropogenic aerosols during a Kosa event over East Asia, *J. Geophys. Res.*, *107*(D7), 4059, doi:10.1029/2001JD000333, 2002.

Uno, I., X.-M. Cai, D. G. Steyn, and S. Emori, A simple extension of Louis method for rough surface layer modeling, *Boundary Layer Meteorol.*, *76*, 395–405, 1995.

Uno, I., H. Amano, S. Emori, K. Kinoshita, I. Matsui, and N. Sugimoto, Trans-Pacific yellow sand transport observed in April 1998: A numerical simulation, *J. Geophys. Res.*, *106*, 18,331–18,344, 2001.

Uno, I., G. R. Carmichael, D. Streets, S. Satake, T. Takemura, J.-H. Woo, M. Uematsu, and S. Ohta, Analysis of surface black carbon distributions during ACE-Asia using a regional-scale aerosol model, *J. Geophys. Res.*, *108*(D23), 8636, doi:10.1029/2002JD003252, in press, 2003.

Walko, R. L., W. R. Cotton, M. P. Meyers, and J. Y. Harrington, New RAMS cloud microphysics parameterization, part I: The single-moment scheme, *Atmos. Res.*, *38*, 29–62, 1995.

Zender, C. S., H. Bian, and D. Newman, Mineral Dust Entrainment and Deposition (DEAD) model: Description and 1990s dust climatology, *J. Geophys. Res.*, *108*(D14), 4416, doi:10.1029/2002JD002775, in press, 2003.

Zobler, L., A world soil file for global climate model, *NASA Tech. Memo*, *87802*, 1986.

G. R. Carmichael, S. Guttikunda, Y. Tang, and J.-H. Woo, Center for Global and Regional Environmental Research, University of Iowa, 402 IATL, Iowa City, IA 52242, USA. (gcarmich@icaen.uiowa.edu; sguttiku@cgrer.uiowa.edu; ytang@cgrer.uiowa.edu; woojh21@cgrer.uiowa.edu)

T. Iida, Graduate School of Engineering, Nagoya University, Chkusa-ku, Nagoya 464-8603, Japan. (t-iida@nucl.nagoya-u.ac.jp)

K. Matsumoto and M. Uematsu, Ocean Research Institute, University of Tokyo, 1-15-1 Minamidai, Nakano-ku, Tokyo 164-8639, Japan. (kiyoshi@ori.u-tokyo.ac.jp; uematsu@ori.u-tokyo.ac.jp)

S. Satake and I. Uno, Research Institute for Applied Mechanics, Kyushu University, Kasuga Park 6-1, Kasuga, Fukuoka 816-8580, Japan. (satake@riam.kyushu-u.ac.jp; iuno@riam.kyushu-u.ac.jp)

D. G. Streets, Argonne National Laboratory, 9700 S. Cass Avenue, Argonne, IL 60439, USA. (dstreets@anl.gov)

H. Tanimoto, Atmospheric Environment Division, National Institute for Environmental Studies, 16-2 Onogawa, Tsukuba, Ibaraki 305-8506, Japan. (tanimoto@nies.go.jp)

Z. Wang, Frontier Research System for Global Change, IGAC-Yokohama, 3173-25 Showa-machi, Kanazawa-ku, Kanagawa, Yokohama 236-0001, Japan. (zifawang@jamstec.go.jp)

J. J. Yienger, Cities for Climate Protection Campaign, ICLEI-US, 15 Shattuck Square, Suite 215, Berkeley, CA 947904, USA. (jyienger@iclei.org)

K. Yoshioka, Shimane Prefectural Institute of Public Health and Environmental Science, 582-1 Nishihamasada, Matsue 690-0122, Japan. (yoshioka-katsuhiro@pref.shimane.jp)